

Enterohemorrhagic *Escherichia coli* infection stimulates Shiga toxin 1 macropinocytosis and transcytosis across intestinal epithelial cells

Valeriy Lukyanenko,¹ Irina Malyukova,¹ Ann Hubbard,² Michael Delannoy,² Edgar Boedeker,³ Chengru Zhu,³ Liudmila Cebotaru,⁴ and Olga Kovbasnjuk¹

¹Department of Medicine, ²Department of Cell Biology, and ⁴Department of Ophthalmology, Johns Hopkins University School of Medicine, Baltimore, Maryland; ³Department of Medicine, University of New Mexico School of Medicine, Albuquerque, New Mexico

Submitted 7 February 2011; accepted in final form 4 August 2011

Lukyanenko V, Malyukova I, Hubbard A, Delannoy M, Boedeker E, Zhu C, Cebotaru L, Kovbasnjuk O. Enterohemorrhagic *Escherichia coli* infection stimulates Shiga toxin 1 macropinocytosis and transcytosis across intestinal epithelial cells. *Am J Physiol Cell Physiol* 301: C1140–C1149, 2011. First published August 10, 2011; doi:10.1152/ajpcell.00036.2011.—Gastrointestinal infection with Shiga toxins producing enterohemorrhagic *Escherichia coli* causes the spectrum of gastrointestinal and systemic complications, including hemorrhagic colitis and hemolytic uremic syndrome, which is fatal in ~10% of patients. However, the molecular mechanisms of Stx endocytosis by enterocytes and the toxins cross the intestinal epithelium are largely uncharacterized. We have studied Shiga toxin 1 entry into enterohemorrhagic *E. coli*-infected intestinal epithelial cells and found that bacteria stimulate Shiga toxin 1 macropinocytosis through actin remodeling. This enterohemorrhagic *E. coli*-caused macropinocytosis occurs through a nonmuscle myosin II and cell division control 42 (Cdc42)-dependent mechanism. Macropinocytosis of Shiga toxin 1 is followed by its transcytosis to the basolateral environment, a step that is necessary for its systemic spread. Inhibition of Shiga toxin 1 macropinocytosis significantly decreases toxin uptake by intestinal epithelial cells and in this way provides an attractive, antibiotic-independent strategy for prevention of the harmful consequences of enterohemorrhagic *E. coli* infection.

transcytosis; foodborne pathogens; diarrhea

ENTEROHEMORRHAGIC *Escherichia coli* (EHEC) is one of the major foodborne pathogens by virtue of its frequency in the United States and worldwide and the severity of the associated illnesses (45, 51). Whereas most EHEC-infected individuals develop watery and bloody diarrhea but recover, up to 20% of these patients develop life-threatening systemic complications that includes hemolytic uremic syndrome (HUS). The US Center for Disease Control and Prevention estimates that the principal EHEC strain O157:H7 causes 73,000 infections and ~60 deaths annually. Recent epidemics such as those related to contaminated leafy green vegetables have increased these totals (7). Most EHEC-induced diseases are attributed to intestinal and systemic spread of Shiga toxins 1 and 2 (Stx1 and Stx2), among which Stx2 is primarily associated with human disease (1, 10). At present there is no conventional therapy for Stx complications. In fact, use of antibiotics and antidiarrheal drugs against EHEC infection has proven to be harmful and shown to increase the risk of developing HUS (51, 55).

Address for reprint requests and other correspondence: O. Kovbasnjuk, Dept. of Medicine, Division of Gastroenterology, 918 Ross Research Bldg., 720 Rutland Ave., Johns Hopkins School of Medicine, Baltimore, MD 21205 (e-mail: okovbas1@jhmi.edu).

To cause intestinal and systemic complications, Stx enter enterocytes, cross the epithelial barrier, and reach the systemic circulation. Previous ideas about the mechanisms of Stx action were dominated by discovery that the glycosphingolipid Gb3 is a receptor for both Stx1 and Stx2 (1, 42). Consequently, early studies focused on characterizing Gb3-mediated retrograde toxin trafficking and assumed that this mechanism applied to human intestinal epithelial cells (IEC) exposed to Stx during EHEC infection. However, recent reports that human enterocytes fail to express detectable amounts of Gb3 either normally or upon EHEC infection (5, 27, 33, 43) have required reevaluation of previous models for Stx-induced intestinal disease. Thus here is a significant gap in our understanding of how Stx interacts with human enterocytes and crosses the intestinal epithelial barrier to cause systemic damage. This gap has clinical consequences: improved understanding of the complex mechanisms of Stx interaction with IEC could aid novel therapeutic strategies for preventing toxin uptake and transcytosis across the intestinal epithelia and in that way prevent HUS and other systemic aspects of the disease.

It is well documented that Stx1 and Stx2 are taken up by enterocytes upon EHEC infection in humans despite the absence/low amount of apical Gb3 receptors in these cells (23, 33). Moreover, experimental evidence showed that toxin transcytosis across the intestinal layer occurs mostly via a cellular route not through tight junctions (2, 32, 46), although transmigration of neutrophils, which takes place in EHEC infection, has been shown associated with paracellular transcytosis of both toxins (20). But the molecular mechanisms of Stx endocytosis and transcellular transcytosis across IEC are virtually uncharacterized.

In this study, we demonstrate that exposure of T84 IEC to EHEC stimulates macropinocytosis (MPC), an actin-dependent endocytic pathway, which significantly increases Stx1 uptake and transcellular transcytosis. Our results suggest that this mechanism might be responsible for toxin transport in disease. We also report that inhibition of MPC at several molecular steps significantly decreases Stx1 uptake and therefore its subsequent transcytosis, raising the possibility of potential targets for therapeutic intervention.

MATERIALS AND METHODS

Reagents and antibodies. Purified Stx1 and Stx2 were prepared as previously described (19, 27). Calyculin A was from Enzo Life Sciences; pirl-1 was from Chembridge; HOE694, and S3226, and recombinant adenovirus containing empty vector were generous gifts from Dr. Mark Donowitz, Johns Hopkins School of Medicine. Antibodies (Abs) were purchased as indicated: mouse anti-Cdc42-GTP

[1:50 dilution for immunofluorescence (IF), NewEast Biosciences]; mouse anti-Cdc42 [dilution 1:250 for Western blot (WB), Santa Cruz]; rabbit anti-NMIIA and MNIIB (WB dilution 1:1,000 for both; Covance); and rabbit anti-phospho-RLC (WB dilution 1:1,000; Cell Signaling), mouse anti-GAPDH (WB dilution 1:1,000; Sigma). Chicken anti-RLC (WB dilution 1:500) was a generous gift from Dr. Jerrold Turner, University of Chicago. Fluorescent secondary Abs for IF (dilution 1:100), phalloidin-AlexaFluor 488 or 568 (IF dilution 1:200), Alexa reactive fluorescent dyes, and Hoechst 33342 were from Invitrogen. Fluorescent secondary Abs for WB (dilution 1:10,000) were from Rockland. Recombinant adenovirus containing Cdc42 (Q61L) was from Cell Biolabs. Cdc42 inhibitory peptide was a generous gift from Dr. Timothy Gomez, University of Wisconsin. All other reagents were from Sigma.

Cell culture. Human colonic epithelial T84 cells (ATCC, Manassas, VA) were grown and maintained in culture in Dulbecco's modified Eagle's medium (DMEM)/Ham's F-12 medium (1:1) supplemented with 10% fetal bovine serum, 100 U/ml penicillin, and 100 µg/ml streptomycin as we previously described (32, 33). All media were obtained from Invitrogen. Cell monolayers (passages 27–45) were grown on polycarbonate inserts with 0.4-µm pore size (Costar, Cambridge, MA) or in plastic six-well plates for 7–14 days. Experiments were performed on confluent monolayers with transepithelial electrical resistances > 1,500 Ω·cm².

Human tissue specimens. Samples of archived frozen human tissue included normal distal and proximal colon ($n = 6$). The samples were coded so no patient identifiers were linked to the specimens. This study was exempted under the Code of Federal Regulations Title 45 Section 46.101(b) by the Hopkins Institution Review Board.

Infection of T84 cells by EHEC strain and treatments with pharmacological agents. Following a published protocol (33), we inoculated T84 cells apically with different concentrations of EHEC strain EDL933 modified to be Stx-negative and incubated them at 37°C in 5% CO₂ for up to 4 h. Fluorescently labeled Stx1-AlexaFluor680 (0.2 µg/ml) was added apically at the time of infection as were inhibitors, such as pirl-1 (0.5 µM), blebbistatin (50 µM), calyculin A (5 nM), Cdc42 inhibitory peptide (40 µg/ml), HOE694 (50 µM), and S3226 (10 µM). After 4 h, the cells were washed three times with cold PBS and fixed for immunofluorescence or lysed in RIPA buffer [1% Triton X100, 0.5% deoxycholic acid, 0.1% SDS, 50 mM Tris-HCl, pH 7.4, 150 mM NaCl containing 0.5 mM Na₃VO₄ and protease inhibitor cocktail 1:1,000 (Sigma P8340)] and centrifuged at 20,000 g at 4°C for 15 min for immunoblotting.

Lentiviral transduction of T84 cell with Cdc42 shRNA constructs. Four sequence-verified short hairpin RNA (shRNA) lentiviral plasmids in a hairpin-pLKO.1 puromycin vector for Cdc42 gene silencing in human cells were obtained from The RNAi Consortium (TRC) library (http://www.broad.mit.edu/genome_bio/trc/rnai.html) through the Johns Hopkins HiT center from Open Biosystems (Huntsville, AL) and were used to generate lentiviral transduction particles as we previously described (33).

Detection of intracellular Stx1 in vitro. The relative fluorescence intensity of Stx1–680 in 150 µg protein in total cell lysates, which corresponds to the intracellular Stx1, was measured in triplicate as we described (33). Alternatively, lysates were subjected to SDS-PAGE and the polypeptides transferred to nitrocellulose membranes. The relative fluorescence intensity of the Stx1–680 band was measured by Odyssey infrared imaging scanner (33) and normalized to the fluorescence intensity of GAPDH obtained by immunoblotting.

Detection of Stx1 transcytosis in vitro. Cells grown on polycarbonate inserts were incubated with 0.2 µg/ml Stx1–680 in the absence (basal transcytosis) or presence of EDL933 bacteria (stimulated transcytosis) for the times indicated in the figure legends. At the end of the incubation, inserts were removed, 100-µl samples of media from the lower chamber containing transcytosed toxin were collected, and the relative fluorescence intensity of Stx1 was measured in triplicate as we previously described (33). Stx1 fluorescence intensity in con-

ditioned media was normalized to fluorescence intensity of conditioned media from cells not infected with EHEC and not exposed to Stx1.

For SDS-PAGE experiments the basal-conditioned media containing transcytosed Stx1-Alexa680 from control and experimental monolayers were concentrated using Amicon Ultra Centrifugal Filter Devices (Millipore) to a final volume of ~150 µl as we have described (29). The supernatant samples (40 µl) were subjected to SDS-PAGE, transferred to nitrocellulose, and analyzed for the presence of fluorescent Stx1 by infrared imaging scanner.

Rabbit model of EHEC-induced colitis. A rabbit cecal model of EHEC-induced colitis was used as described (33, 47). Briefly, the enteroadherent rabbit *E. coli* pathogen RDEC-1, which forms attaching/effacing (A/E) lesions similar to those in EHEC-infected humans, was transduced with Stx1-converting phage ΦH19A to express Stx1 and given by gavage. To discriminate between Stx1-specific intestinal epithelial changes and the changes related to enteric colonization, we infected male New Zealand White rabbits (2.5–5 kg, Myrtle's Rabbitry, Thompsons Station, TN) with 10¹⁰ RDEC-1 ($n = 2$), 10¹⁰ Stx1-producing RDEC-H19A ($n = 3$) or PBS ($n = 2$). Experiments with animals were performed at the University of New Mexico, School of Medicine using a protocol approved by the University of New Mexico Animal Use Committee. Three days after challenge, animals were euthanized, and cecal tissues from control and experimental rabbits were rinsed with ice-cold PBS, opened along the mesenteric border, snap frozen in liquid nitrogen, and stored at –80°C until further use. We found that at *day 3* after inoculation, RDEC-H19A-infected rabbits already showed the disease symptoms (liquid stool, lower weight, etc.) compared with those inoculated with the nontoxicogenic strain or PBS (33). These changes preceded the ischemia/inflammatory changes detected at *day 7* (edema, neutrophil transmigration, etc.).

Immunofluorescence. Rabbit tissue and T84 cell immunostaining was performed as we previously described (33). Briefly, for Cdc42-GTP immunostaining, 10-µm sections of frozen cecal tissues from rabbits infected with RDEC-H19A bacteria were fixed in 3% formaldehyde in PBS for 30 min, washed extensively in PBS, permeabilized with 0.1% saponin, and blocked with 2% BSA and 15% FBS for 45 min. Sections were incubated with primary antibodies at room temperature for 1 h, washed three times in PBS, and incubated with fluorescently labeled secondary antibodies phalloidin for F-actin and Hoechst for nuclear staining, for an additional 1 h, washed again, immersed in gel mount, and mounted on glass slides for confocal microscopy.

Detection of Stx2 binding sites in human colonic tissue was done as we described (27). Briefly, cryosections of normal human colonic tissue from six individuals were fixed, permeabilized, and blocked as described above. Sections were incubated with Stx2-Alexa568 and B-subunit of cholera toxin (CTB)-Alexa 488 and Hoechst for 1 h, washed again, immersed in gel mount, and covered with coverslips for confocal microscopy.

For cell immunofluorescence experiments, confluent T84 monolayers grown on filters were fixed with 3% formaldehyde in PBS for 10 min, washed extensively in PBS, permeabilized as described above for 30 min, and then incubated with primary and fluorescently labeled secondary antibodies, rinsed, and mounted as described above.

Fluorescence confocal imaging of tissue and cells was performed using Zeiss 510 LSM. Eight- or twelve-bit fluorescence images of confocal optical 0.4-µm sections were collected for further qualitative and quantitative analysis using MetaMorph software (Roper Industries, Marlow, UK).

For SR-SIM images, T84 cells (infected and uninfected) grown and treated as above and labeled with phalloidin-AlexaFluor 488 were mounted on slides using Vectashield mounting medium (Vector Laboratories, Burlingame, CA). The images were obtained using super resolution SIM ELYRA PS.1 system by Zeiss (Jena, Germany).

SEM and TEM imaging. For scanning electron microscopy (SEM), T84 cells grown on filters were rinsed in $1 \times$ PBS for 1 min and then fixed in solution containing 2.0% paraformaldehyde (PFA), 2% glutaraldehyde (GA), 0.1 M sodium cacodylate, 1% sucrose, and 3 mM CaCl_2 , pH 7.42, overnight at 4°C . After the buffer rinse, samples were postfixed in 2% osmium tetroxide and 0.1 M sodium cacodylate for 1 h on ice in the dark. After a brief $\text{D-H}_2\text{O}$ rinse cells were then placed in 2% uranyl acetate for 1 h at room temperature in the dark. After en bloc staining, cells were dehydrated through a graded series of ethanol transferred to a 1:1 mixture of ethanol HMDS (Polysciences) and then passed through two changes of pure HMDS. Drying agent was decanted, and samples were placed in a dessicator with a 15-psi vacuum overnight. Filters were attached to aluminum stubs via carbon sticky tabs (Pella) and coated with 20 nm of AuPd with a Denton Vacuum Desk III sputter coater. Stubs were viewed and digital images captured on a Leo 1530 FESEM operating at 1–3 kV.

For transmission EM (TEM), rabbit cecal tissue samples (~ 3 mm) were fixed in solution containing 2% GA, 2% PFA, 0.1 M sodium cacodylate, 3 mM CaCl_2 , pH 7.2 overnight at 4°C . After the buffer rinse, samples were postfixed in 2% osmium tetroxide in 0.1 M sodium cacodylate for 1 h on ice in the dark. After a brief $\text{D-H}_2\text{O}$ rinse tissue samples were placed in 2% uranyl acetate for 1 h at room temperature in the dark. After en bloc staining, tissue samples were dehydrated through a graded series of ethanol to 100%, transferred

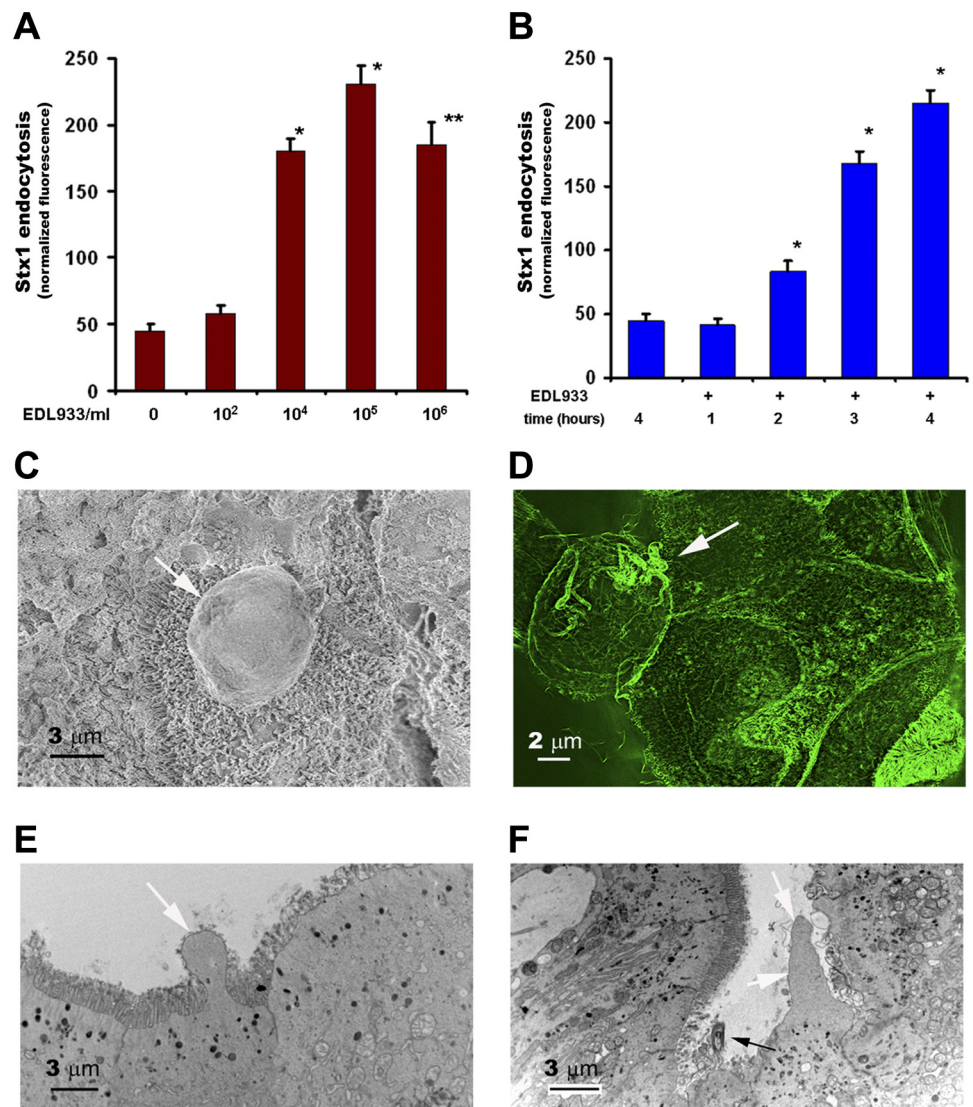
through propylene oxide, embedded in Eponate 12 (Pella), and cured at 60°C for 2 days. Sections were cut on a Riechert Ultracut E with a Diatome Diamond knife. Sections of 80 nm were collected on formvar-coated 1×2 mm copper slot grids and stained with uranyl acetate followed by lead citrate. Grids were viewed on a Hitachi 7600 TEM operating at 80 kV and digital images captured with an AMT 1 K \times 1 K CCD camera.

Statistical analysis. Values are presented as means \pm SE and the number (n) of independent preparations. Statistical significance was determined using Student's unpaired t -test and P value < 0.05 was considered significant.

RESULTS

EHEC infection stimulates Stx1 endocytosis in IEC. We tested the effect of EHEC infection on Stx1 uptake by IEC. For these experiments T84 cells were infected with increasing concentrations of EDL933 bacteria in the presence of fluorescently labeled Stx1 ($0.2 \mu\text{g/ml}$) applied apically. The relative amount of endocytosed Stx1 was measured 4 h after infection in total cell lysates and compared with the amount of Stx1 taken up by uninfected cells. Increasing the bacterial concentration resulted in an increase in Stx1 uptake (Fig. 1A). At

Fig. 1. Infection of intestinal epithelial cells (IEC) with enterohemorrhagic *Escherichia coli* (EHEC) significantly increases Shiga toxin 1 (Stx1) uptake by stimulation of macropinocytosis (MPC). **A:** uptake of Stx1-Alexa680 by T84 cells was stimulated by increasing concentrations of EDL933. **B:** 10^4 EDL933/ml significantly increased Stx1-Alexa680 uptake over time. $n \geq 6$. The amount of endocytosed toxin in **A** and **B** was measured in total cell lysates in triplicates by fluorescent plate reader and normalized to the protein concentrations ($n \geq 6$). *Significant compared with uninfected cells; **significant compared with 10^5 EDL933/ml. **C:** scanning electron microscopy (SEM) of T84 cells infected with EDL933 shows apical bleb (arrow) in places without attached bacteria. **D:** SIM image of EDL933-infected T84 cells and immunostained with phalloidin-AlexaFluor 488 demonstrates the F-actin nature of the apical bleb (arrow). Image represents the superimposition of 6 optical sections with $1\text{-}\mu\text{m}$ step. **E** and **F:** transmission EM (TEM) images of cecal epithelium from rabbits infected for 3 days with RDEC-H19A bacteria show that the apical blebs (white arrows in **E** and **F**) appear in places without and with attached bacteria (black arrow in **F**).



bacterial concentration $\geq 10^6$ EDL933/ml (Fig. 1A) this effect on Stx uptake was reduced due to significant increase in cell death compared with control ($16\% \pm 6$, $n = 4$, $P < 0.05$) as detected by the propidium iodide incorporation into the nuclei. To confirm that bacterial infection modulated toxin uptake in T84 cells, we measured Stx1 endocytosis over time at a single 10^4 EDL933/ml concentration that did not cause significant cell death 4 h after infection. Stx1 uptake increased in a time-dependent manner in EHEC-treated versus uninfected cells (Fig. 1B). Thus we conclude that bacterial infection stimulates Stx1 uptake by IEC.

EHEC infection causes formation of actin-based macropinocytic blebs at the apical surface of IEC in vitro and in vivo. We have previously shown that in Gb3 receptor-deficient intestinal epithelial T84 cells, the basal uptake of Stx1 occurs through an actin-dependent mechanism, which we speculated to be MPC (32). MPC is defined as actin-driven, clathrin- and caveolin-independent endocytosis that results in the internalization of fluid and high molecular weight cargo into large irregular vesicles with diameters up to $10 \mu\text{m}$ (35, 50). The rate of MPC in IEC is generally low but increases significantly upon stimulation by growth factors, protein kinase C, and the nonreceptor tyrosine kinase Src, etc. (12, 24, 36). We have shown that pharmacological stimulation of MPC significantly increased Stx1 endocytosis in T84 cells (33), whereas treatment of T84 cells with cytochalasin D (CytD) significantly inhibited basal Stx1 MPC in T84 cells (32).

We next tested whether the treatment of EHEC-infected T84 cells with $1 \mu\text{M}$ CytD for 4 h affects Stx1 uptake. Stx1 relative fluorescence intensity in total cell lysates fell from 4.5 ± 0.3 in cells without CytD treatment to 2.4 ± 0.4 in CytD-treated cells ($P = 0.01$, $n = 6$), indicating that EHEC-induced Stx1 uptake is an actin-dependent process.

Knowing that EHEC upon attachment and effacement (A/E) to the enterocyte brush border causes a substantial actin rearrangement (6, 10), we speculated that EHEC might induce actin remodeling both locally at sites of A/E and also globally. Thus we have tested the hypothesis that EHEC-induced actin remodeling stimulates MPC, which results in increased Stx1 uptake.

MPC is induced by the activation of plasma membrane-connected actin, which leads to ruffle formation. The macropinocytic ruffles can take different forms, such as lamellipodia, circular ruffles, and, in some cases, large (up to $10 \mu\text{m}$) plasma membrane blebs (35). Examination of T84 cells by confocal microscopy showed that EDL933 infection caused both apical and basolateral actin rearrangement and apical actin ruffling (supplemental Fig. S1, A–D). SEM showed substantial rearrangement of the apical surface leading to the disappearance of microvilli and formation of so-called macropinocytic blebs (Fig. 1C). Super resolution structural illumination microscopy (SR-SIM) images confirmed the F-actin nature of these blebs in T84 cells (Fig. 1D). Importantly, the apical blebs appeared in locations that lacked A/E bacteria (Fig. 1C), suggesting that blebs were not a direct consequence of localized bacterial attachment (supplemental Fig. S1E).

To test whether appearance of apical blebs was a characteristic feature of EHEC-induced disease, we used TEM to compare cecal tissue from rabbits infected for 3 days with Stx1-producing RDEC-H19A bacteria to comparable samples from PBS-treated rabbits. RDEC-H19A infection was associ-

ated with apical blebbing of cecal epithelial cells (Fig. 1E), morphologically similar to these detected in EHEC-infected T84 cells. Analysis of in vivo model shows that the blebs were formed randomly at the sites without attached bacteria (Fig. 1E) and at some distance from the attached bacteria (Fig. 1F), similarly to our in vitro finding.

Macropinosomes carry Stx1 into and across IEC. It has been shown (35) that retraction of macropinocytic blebs causes the uptake of Vaccinia virus through formation of actin-coated macropinosomes. We examined Stx1 distribution in EDL933-infected T84 cells and found that toxin was present inside of large actin-coated apical vesicles, which by definition resemble macropinosomes (Fig. 2A).

We followed the fate of internalized toxin in T84 cells and found that the majority of these actin-coated vesicles did not release the cargo intracellularly over the 4 h of experimental time but rather delivered actin-coated Stx1 to the basal surface of T84 cells (Fig. 2B). To test whether this apical-to-basal Stx1 transport contributes to toxin transcytosis across the T84 monolayers, we measured the relative amount of Stx1 in basolateral conditioned media from infected versus uninfected

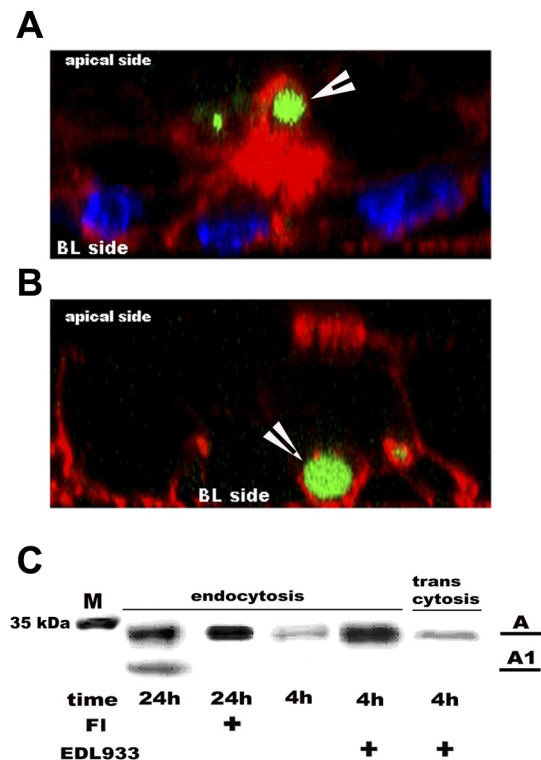


Fig. 2. Stx1 taken up by MPC is transcytosed across the T84 cells in holotoxin form. **A**: XZ projection through an EHEC-infected T84 cell shows apical F-actin bleb (red) that takes up Stx1 (green). **B**: XZ projection through EHEC-infected T84 cells with internalized Stx1 shows that Stx1 (green) is transported to the basolateral side of the cells inside the F-actin-coated macropinosomes (red). F-actin, red by phalloidin-AlexaFluor 568; Stx1, green by conjugation to AlexaFluor 488; nuclei, blue by Hoechst. White arrows in **A** and **B** indicate the green Stx1-containing vesicles coated with red F-actin. **C**: SDS-PAGE shows the relative distribution of Stx1A and cleaved Stx1A1 in total cell lysates (endocytosis) and in basal conditioned media (transcytosis) from T84 cells incubated with Stx1 over indicated time in the presence of $50 \mu\text{M}$ furin inhibitor decanoyl-RVVR-CMK or in EHEC-infected cells. M indicates the corresponding molecular mass marker on a gel. Stx1 taken up by MPC is not cleaved inside the T84 cells 4 h later. Transcytosed toxin collected from basal conditioned media 4 h after EHEC infection is also not cleaved.

cells. MPC of Stx1 at the apical surface significantly increased the amount of toxin detected in the basal medium 4 h after infection. Specifically, the presence of apical bacteria resulted in significantly more transcytosed Stx1–680 than when no bacteria were added (Stx1 normalized fluorescence intensity: 8.3 ± 0.5 vs. 3.7 ± 0.4 , $P < 0.05$, $n = 12$). To further determine whether the transcytosed toxin could have been intracellularly activated, we analyzed the mobility of the Stx form(s) by SDS-PAGE. To generate enzymatically active toxin, the catalytic A-subunit of Stx1 (M_r 32kDa) must be cleaved into two fragments, an active A1 form (M_r 27.5kDa) and a small A2 (M_r 4.5 kDa). Furin, a membrane-associated serine endoprotease, has been shown to activate the toxin in endosomes/trans-Golgi, whereas calpain, a cysteine protease, cleaves Stx1 in the cytoplasm (13, 28). Therefore, detection of the cleaved A1 fragment of Stx1 in total cell lysates or in the basal conditioned media would indicate that internalized Stx had been sorted into an endocytic compartment or released into the cytosol. However, 4 h after EDL933 infection of T84 cells, cellular Stx1 was mostly present in its holotoxin form, with the A1 fragment below detection levels (Fig. 2C), as was the transcytosed Stx1 from basolateral conditioned media. This result suggests that toxin-bearing actin-coated vesicles neither fused with furin-positive compartments nor allowed release of the toxin directly into the cytosol. However, in agreement with published results (43), exposure of uninfected T84 cells to toxin for 24 h resulted in furin-mediated cleavage of intracellular Stx1 to the A1 form, a process that was inhibited by a known furin inhibitor (Fig. 2C).

Taken together, these results demonstrate that early in EDL933 infection, MPC leads to Stx1 uptake and transcellular

transcytosis of the holotoxin, thus providing a route for the holotoxin's systemic dissemination. Clearly, inhibition of EHEC-induced MPC could be an effective means to interfere with toxin-induced systemic diseases. This possibility prompted us to further characterize the molecular mechanism(s) of toxin MPC.

Stx1 uptake by EHEC-induced macropinocytosis is myosin II dependent. Nonmuscle myosin II (NMII), an actin-based motor protein, has been implicated in MPC that is induced by a variety of stimuli, including viruses, growth factors, etc. in different cell types (9, 22, 35). Therefore, we tested its role in EHEC-induced MPC of Stx1 using reagents that modulate its activity. Blebbistatin is a specific pharmacological inhibitor of NMII ATPase activity (48, 54), and calyculin A at low concentrations specifically inhibits myosin light chain phosphatase (54), thus increasing NMII activity. We found that blebbistatin (50 μ M) significantly inhibited EHEC-induced Stx1 uptake (Fig. 3, A and B), whereas calyculin A (5 nM) significantly increased its uptake, indicating that NMII was involved in Stx1 MPC. NMII activity requires phosphorylation of regulatory light chain RLC (34). To confirm that NMII was activated in T84 cells after EDL933 infection, we measured the extent of RLC phosphorylation and found a significant increase (Fig. 3C).

Among three isoforms of NMII (A, B, and C), NMIIA and B but not C are expressed in T84 cells (21). We determined the relative amounts and distributions of both isoforms in control conditions and after 4 h of infection. NMIIA was significantly upregulated after exposure to bacteria (Fig. 3D) but not NMIIIB (Fig. 3E). The NMIIA-to-GAPDH ratio in EDL933-infected cells was 2.1 ± 0.6 ($P = 0.04$, $n = 10$) when normalized to that

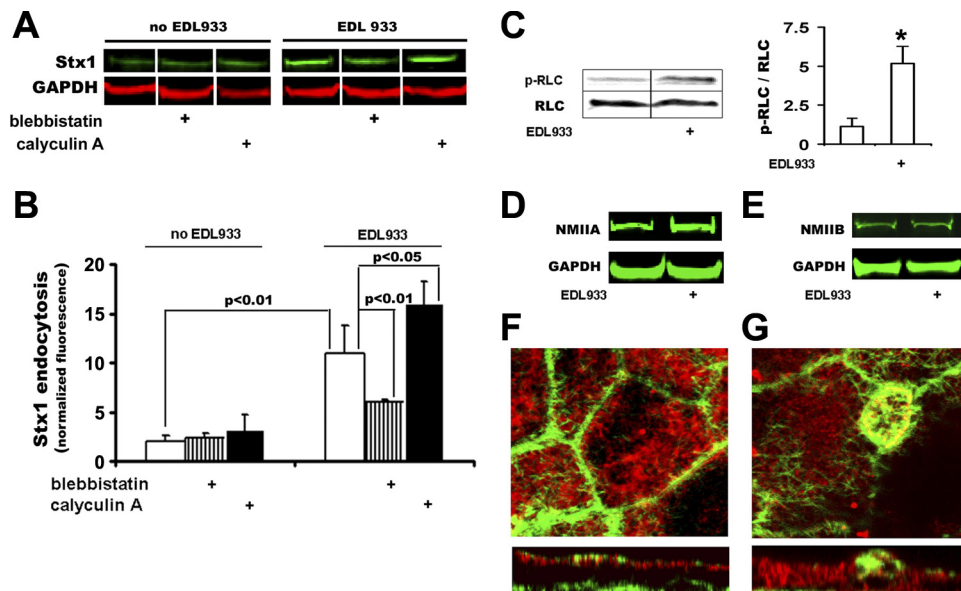


Fig. 3. Nonmuscle myosin II (NMII) plays a role in EHEC-stimulated Stx1 MPC. **A**: representative immunoblot of Stx1-Alexa 680 and GAPDH from infected and uninfected T84 cells that were treated or not with 50 μ M blebbistatin or 5 nM calyculin A for 4 h. **B**: treatments of T84 cells with either 50 μ M blebbistatin or 5 nM calyculin A for 4 h affect EHEC-induced Stx1 MPC; $n \geq 3$ per each condition. **C**: immunoblot of T84 total cell lysates shows increase in RLC phosphorylation upon EHEC infection with corresponding quantification of RLC phosphorylation. *Significant compared with uninfected cells ($P < 0.05$; $n = 5$). **D**: representative immunoblot of NMIIA shows the increase in the NMIIA amount in cells infected for 4 h with EDL933 compared with control uninfected cells. **E**: representative immunoblot of NMIIIB shows no changes in the NMIIIB amount in cells infected for 4 h with EDL933 compared with control uninfected cells. **F–G**: NMIIA is present in F-actin apical blebs induced by EDL933. Representative XY optical section through the apical region with corresponding XZ projection of T84 cells uninfected (**F**) or infected (**G**) with EDL933 for 4 h and immunostained against NMIIA with F-actin; green by phalloidin-AlexaFluor488 and to visualize NMIIA. The pattern of NMIIA overlaps with the pattern of F-actin at the perimeter of the bleb.

of control cells. Furthermore, the intracellular distributions of NMIIA in uninfected versus infected cells were very different. In uninfected cells, NMIIA was exclusively subapical (Fig. 3F and supplemental Fig. S2A), whereas in infected cells it was present throughout the cells (Fig. 3G and supplemental Fig. S2B). Importantly, NMIIA was present all through the apical macropinocytic blebs and concentrated at the perimeter of the blebs where it colocalized with F-actin [yellow color in Fig. 3G (XY plane) and white ring at the bleb perimeter in supplemental Fig. S. 2B (XY plane), which follows the F-actin pattern in the bleb]; $73.1\% \pm 7.1$ of NMIIA colocalized with F-actin in these blebs, whereas only $9.9\% \pm 2.5$ of NMIIA colocalized with the F-actin through the rest of the cells.

The distribution of NMIIIB was also altered in EHEC-infected compared with control cells, but this isoform was not present in F-actin blebs (supplemental Fig. S3, A and B). Therefore, it seems that only NMIIA is involved in formation of EHEC-induced actin blebs in T84 cells, and its inhibition significantly decreased Stx1 uptake by EHEC-stimulated MPC.

Cdc42 is necessary but not sufficient for MPC of Stx1. Macropinosome formation usually requires membrane ruffling. It is well established that Rho GTPases, including Cdc42, are responsible for the triggering of membrane ruffles by activating effectors of actin polymerization, stability, and turnover (15, 56). For example, Cdc42 plays a role in ruffling during *Salmonella typhimurium* induced MPC in dendritic cells (14). It is also involved in MPC of several types of viruses (35). Consequently, we tested the role of Cdc42 in EHEC-stimulated MPC of Stx1.

EHEC infection led to a significant increase in the amount of Cdc42 in T84 cells after 4 h (supplemental Fig. S4B). Specifically, the Cdc42-to-GAPDH ratio in treated cells was 2.6 ± 0.3 -fold increased ($P < 0.005$, $n = 17$) over that in control cells, suggesting Cdc42 involvement in Stx1 MPC. To confirm the role of Cdc42 in Stx1 uptake by MPC, we used both pharmacological and molecular approaches. Inhibition of Cdc42 activity by either pirl-1, a specific blocker of nucleotide exchange on Cdc42 (37), or a cell-permeable Cdc42-specific inhibitory peptide (39, 53) significantly decreased Stx1 uptake in EHEC-infected cells (Fig. 4A).

We also employed a knockdown (KD) approach to test the role of Cdc42 in MPC using three different shRNA sequences, as we previously described (Ref. 33 and supplemental Fig. S4A). Cdc42 KD virtually abolished the EHEC-stimulated Stx1 uptake (Fig. 4B). In contrast, cells infected with scrambled shRNA that did not inhibit Cdc42 (Ref. 33 and supplemental Fig. S4A) behaved like a wild type (Fig. 4B). Examination of Cdc42 KD cells by SEM showed a reduction in the number of microvilli (supplemental Fig. S5A), which did not significantly affect bacterial attachment (supplemental Fig. S5B). However, the number and the size of apical blebs in EHEC-infected Cdc42 KD T84 cells (supplemental Fig. S5C) were less, indicating that defects in bleb formation might be responsible for the inhibition of Stx1 uptake in the presence of bacteria.

Conversely, transduction of T84 cells with recombinant adenovirus encoding constitutively active Cdc42 (Q61L) (16) significantly increased Stx1 uptake upon EHEC infection (Fig. 4C). These data show that Cdc42 is necessary for EHEC-stimulated MPC of Stx1. However, constitutively active Cdc42 (Q61L) in the absence of bacteria did not stimulate Stx1 uptake

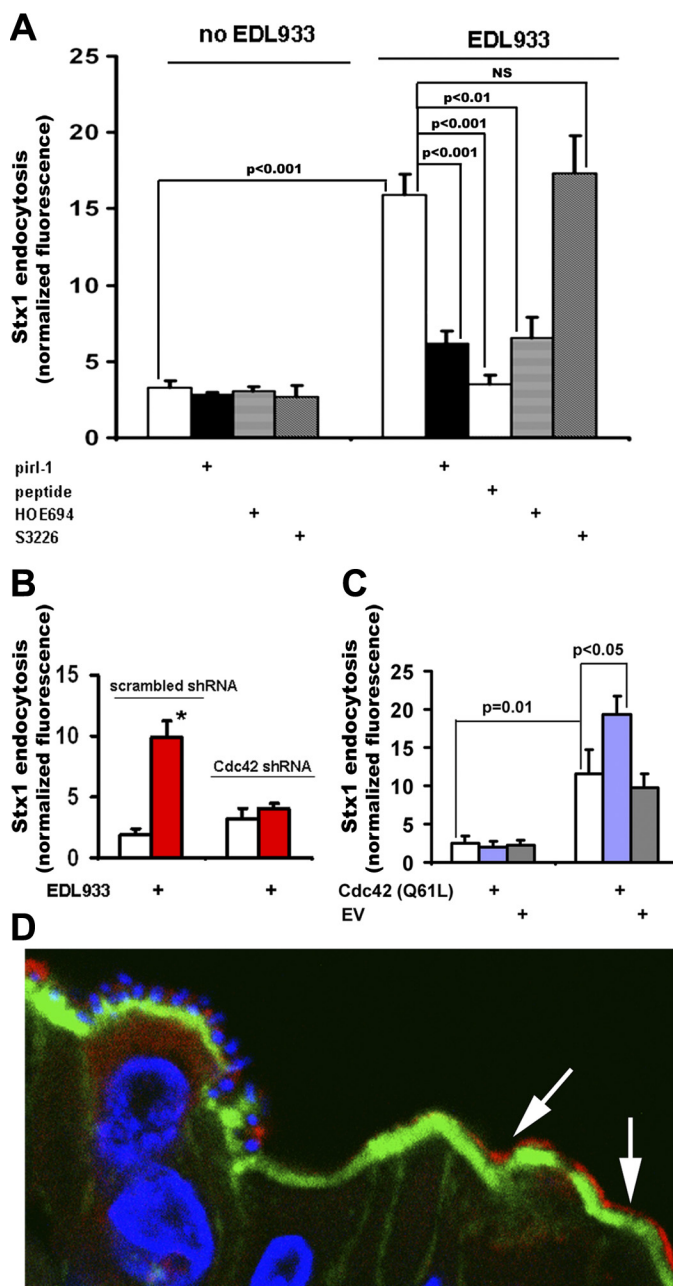


Fig. 4. Cdc42 is necessary for EHEC-induced MPC in vitro and in vivo. *A*: pharmacological inhibition of Cdc42 activity decreases EHEC-stimulated Stx1 uptake in T84 cells; $n \geq 3$. NS, nonsignificant. *B*: Cdc42 KD virtually abolishes the EHEC stimulation of Stx1 uptake. Cdc42KD data represent the combined data from 3 different short hairpin RNA (shRNA) constructs. *Significant compared with control (uninfected T84 cells transduced with lentivirus containing scrambled shRNA; $P < 0.05$; $n = 8$). *C*: constitutively active Cdc42 enhances the EHEC effect on Stx1 endocytosis but is not sufficient to stimulate MPC itself. EV, empty vector; $n \geq 3$ for each condition. *D*: Cdc42 was active (red by anti-Cdc42-GTP Abs, with secondary AlexaFluor 568) in subset of rabbit cecal epithelial cells that often did not have attached bacteria; attached RDEC-H19A bacteria and T84 cell nuclei, blue by Hoechst (33); apical F-actin, green by phalloidin-AlexaFluor 488.

(Fig. 4C), indicating that Cdc42 activation is not sufficient to trigger toxin MPC in T84 cells.

MPC is sensitive to Na/H exchange (NHE) inhibitors, including amiloride, its derivatives, and HOE-694. The mecha-

nism is thought to be due to a decrease in cytosolic pH, which affects both actin assembly and activation of small GTPases, including Cdc42 (26). T84 cells express predominantly two isoforms of plasma membrane Na/H exchanger, basolateral NHE1 and apical NHE2 (4, 17). Inhibition of both by HOE-694 (50 μ M) significantly decreased Stx1 endocytosis in EHEC-infected cells (Fig. 4A). This decrease in Stx1 uptake was due to specific inhibition of NHE function, because treatment of T84 cells with 10 μ M S3226 (44), a specific inhibitor of the NHE3 isoform, which is not expressed in T84 cells, did not influence EHEC-stimulated Stx1 uptake (Fig. 4A).

Because Cdc42 appears to play an important role in EHEC-stimulated Stx1 uptake in vitro, we tested whether activation of Cdc42 was relevant to the EHEC-induced disease using an animal model. Examination of cecal epithelial tissue from rabbits infected either with Stx1-producing RDEC-H19A strain or with nontoxicogenic RDEC-1 bacteria, showed active plasma membrane-bound Cdc42 in the subsets of enterocytes, suggesting that activation of Cdc42 is a molecular event in EHEC infection in vivo (Fig. 4D). Cdc42 plays an important role in EHEC A/E to the apical surface of enterocytes (41, 52). Thus EHEC through type 3 secretion system (T3SS) translocate the effector protein Map to modulate the Cdc42 activity, which is necessary for actin pedestal formation. However, in our in vivo model the active GTP-bound Cdc42 appeared not only in places of bacterial A/E but also in subpopulations of enterocytes having no detectable bacteria nearby (Fig. 4D). This result suggests a potential role for Cdc42 activation in processes beyond the bacterial attachment, including MPC.

We conclude that activation of Cdc42 is a necessary step in the EHEC-stimulated MPC of Stx1, and its inhibition leads to a significant decrease in Stx1 uptake and transcytosis.

Cross-talk between NMII and Cdc42 in EHEC-stimulated macropinocytosis. NMII controls the activation of small GTPases, including Cdc42, in migrating cells (9, 30). Thus we wondered whether NMIIA activation was upstream of Cdc42 activation in EHEC-stimulated MPC. We tested this possibility by analyzing the effects of inhibitors on either NMII or Cdc42 expression/activation in the presence of EHEC. The Cdc42 inhibitor pirl-1 had no effect on the relative NMIIA amounts either in uninfected cells or in the EDL933-infected cells. Likewise, neither Cdc42 KD nor expression of the constitutively active mutant of Cdc42 changed the EHEC-induced increase in the NMIIA. However, inhibition of NMII activity by blebbistatin significantly impaired the bacteria-induced Cdc42 upregulation (10.5 ± 1.0 in infected cells vs. 6.7 ± 2.4 in infected cells plus blebbistatin, $P = 0.03$, $n = 3$). Taken together, these data suggest that Cdc42 works downstream of NMII in EHEC-induced formation of macropinocytic blebs.

EHEC infection stimulates Stx2 endocytosis in IEC. Although Stx1 and Stx2 are structurally and functionally similar, several clinical studies have reported that bacteria producing only Stx2 or Stx2 plus Stx1 are more frequently associated with disease than Stx1-producing strains (1, 19, 45). We speculated that it might be due to differences in Stx1 and Stx2 uptake mechanisms by normal human enterocytes; namely, Stx1 does not bind to enterocytes due to the absence of Gb3 receptor on these cells (5, 27, 33, 43), whereas Stx2 might bind to enterocytes (57). This receptor-mediated Stx2 endocytosis might provide a more efficient route for Stx2 uptake by enterocytes and thus might lead to more severe damage com-

pared with Stx1. In this scenario, the role of EHEC infection in Stx2 uptake might not be important. Thus we first determined whether Stx2 binds to normal human colonocytes using cryosection samples of normal human colonic tissue treated with fluorescently labeled Stx2. No Stx2 binding to normal human colonocytes was detected (Fig. 5A), as has been previously reported (43). Stx2 does bind to subset of cells in lamina propria, which again confirms the previous observations (43). We have used the B-subunit of CTB, which binds to glycosphingolipid GM1 to confirm the preservation of glycosphingolipids in our preparation (Fig. 5B) and detected the bound CTB in both surface and crypt colonocytes, as well as in cells populating the lamina propria, which is in agreement with published data (27).

Based on these findings, we speculate that EHEC infection might play a role in Stx2 uptake by IEC. We next tested the effect of EHEC infection on Stx2 uptake by IEC. For these experiments T84 cells were infected with 10^4 EDL933/ml in the presence of increasing apical concentrations of fluorescently labeled Stx2-Alexa790 (Fig. 5C). The relative amount of endocytosed Stx2 was measured 4 h after infection in total cell

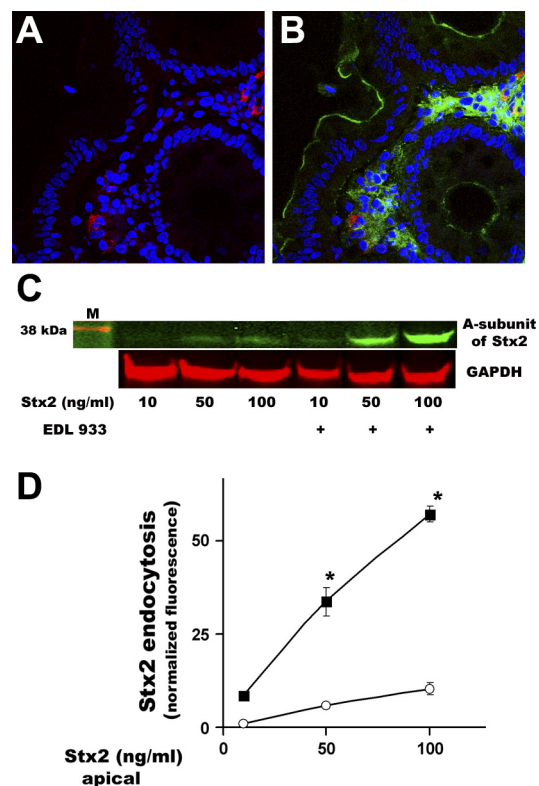


Fig. 5. Stx2 does not bind to normal human colonocytes and its uptake is stimulated by EHEC infection in T84 cells. **A** and **B**: representative projection through 5 confocal optical sections (step 0.5 μ m) of normal human colonic tissue immunostained with Stx2-Alexa 568 (red) (**A**) and colabeled with CTB-Alexa 488 (green) (**B**); nuclei, blue by Hoechst. No Stx2 binding was detected in human colonocytes, but Stx2 (red) labeled some cells in lamina propria which its nature has to be identified. In contrast, cholera toxin B (CTB) (green) binds to the human surface and crypt colonocytes. **C**: representative immunoblot of Stx2-Alexa 790 and GAPDH from infected (10^4 EDL933/ml) and uninfected T84 cells and exposed apically to different Stx2 concentrations for 4 h. **D**: corresponding quantification of Stx2 uptake by uninfected (control, open circles) T84 cells or infected for 4 h with 10^4 EDL933/ml (black squares); *Significant compared with corresponding control conditions, $P < 0.01$; $n = 3$ per each condition.

lysates and compared with the amount of Stx2 taken up by uninfected cells (Fig. 5, C and D). Increasing the toxin concentration resulted in an increase in Stx2 uptake in both control uninfected and infected cells. However, EDL933 significantly increased Stx2 uptake compared with that in control cells for each given toxin concentration (Fig. 5, C and D). Linear dependence between the increase in apical toxin concentration and the increase in Stx2 endocytosis indicates a receptor-independent process, potentially MPC (Fig. 5D). Thus we conclude that Stx2 uptake by IEC is significantly facilitated by EHEC infection, similarly to Stx1 endocytosis.

DISCUSSION

In this study, we have demonstrated that Stx1 uptake by IEC, which lack Gb3 receptors, occurs by MPC and requires infection by EHEC to stimulate MPC. Recent work characterizing the molecular mechanisms of MPC in a variety of cell types exposed to different stimuli has elucidated the criteria for defining MPC (11, 25, 49). EHEC-induced MPC fits these criteria: it requires actin remodeling for macropinocytic bleb formation, for which NMII and the small GTPase Cdc42 are necessary components. The phenotype of EHEC-induced macropinocytic blebs closely resembles these induced by Vaccinia virus (35).

Our results also show that the appearance of macropinocytic blebs did not correlate with the location of A/E bacteria *in vitro* or *in vivo*. This is in good agreement with many earlier observations showing no direct correlation between actin polymerization, pedestal formation, effacement of the brush-border microvilli, or EHEC colonization (41). Furthermore, reports that EDL933 infection of T84 cells (46) and EHEC O157:H7 infection in mice (40) caused disruption of microvilli throughout the apical surface and not only at sites of bacterial A/E are in agreement with our results, which show that EHEC infection rearranges cellular actin on a global scale. Thus the appearance of macropinocytic blebs might be a result and a by-product of this rearrangement.

Our results also show that EHEC-stimulated MPC significantly increased Stx1 uptake within 4 h of exposure, which occurred before the significant bacteria-induced damage to T84 cells. Under these experimental conditions, Stx1 was first detected inside actin-coated apical macropinosomes and subsequently delivered to the basal media in a holotoxin form, indicating the virtual absence of macropinosome fusion with endocytic vesicles in 4 h where sorting of cargo into recycling or degradation pathways would expose Stx1 to cleavage by specific proteases. Although it has been shown that transmigration of neutrophils is associated with an increase in paracellular transcytosis of both toxins (20), the transmigration of polymorphonuclear leukocytes across the lung epithelial cells showed no breaching the integrity of the epithelial barrier for 10 kDa dextran (8). Thus more studies have to be done to determine the role of paracellular pathway in Stx dissemination. Moreover, in our 3-day rabbit model of EHEC infection, no neutrophil transmigration was detected, despite the animals developed loose stool, weight loss, and brush-border damage (33). It remains possible that paracellular toxin movement associated with neutrophil transmigration takes place at the later stages of EHEC-induced disease. Thus we propose that

MPC is likely to be a major route for systemic spread of toxin at the earlier stage of human EHEC infection.

We have also shown here that EHEC infection significantly stimulates the uptake of Stx2 by IEC, a toxin that is associated with severe human disease compared with Stx1. In the absence of Stx2 receptors in normal human enterocytes (43 and Fig. 5, A and B), this EHEC-induced endocytic pathway (probably MPC) might play an important role in uptake of Stx2 in human disease. It has been previously shown that Stx1 and Stx2 use separate routes for translocation across Gb3-positive Caco-2 monolayers (20). Thus it has to be determined in Gb3-negative cell models as well as *in vivo* whether Stx2 and Stx1 share the same EHEC-induced macropinocytic vesicles and whether the regulation of Stx1 and Stx2 MPC and transcytosis is similar or different. Our analysis (33) of Stx1 and Stx2 distribution in human intestinal tissue samples collected during the 1993 *E. coli* O157:H7 epidemic in the western United States from several EHEC-infected patients showed both toxins present in villus/surface and crypt epithelial cells as well as in lamina propria. Moreover, some vesicles carried single toxin, whereas other carried both toxins. But neither toxin showed a distinct binding pattern at the apical surface of enterocytes, supporting our and others findings (43) that neither Stx1 nor Stx2 bind to the receptor(s) at the apical surface of enterocytes. Interestingly, the variability in the relative amount of Stx2 between the samples was greater than in a relative amount of Stx1, indicating that severity of disease may correlate with the amount of taken up and transcytosed Stx2 by enterocytes.

EHEC are not the only bacteria able to induce MPC that results in cargo transcytosis. The short-term infection of human ileal tissue with *Yersinia pseudotuberculosis* caused the transcellular transcytosis of nanoparticles by villus enterocytes via MPC (38). These data together with our observations suggest a novel mechanism of intestinal barrier dysfunction driven by bacterial infections.

What EHEC factors are responsible for stimulating MPC? Application of apical conditioned media from T84 cells infected for 4 h with EDL933 strain onto naïve monolayers did not duplicate the bacterial effect on the Stx1 uptake. It is well established that the bacterial locus of enterocyte effacement (LEE)-encoded T3SS is necessary for formation of EHEC-induced A/E lesions. However, EHEC secreted protein FU (EspFu), the only EHEC-specific effector required for actin polymerization, is encoded outside of the LEE (41). Thus the role of T3SS and other secretion systems in the stimulation of MPC needs to be addressed in the future.

Regardless of the mechanism of MPC stimulation, its inhibition at discrete steps in the chain of EHEC-stimulated macropinocytic events might serve as potential therapeutic targets to decrease the severity of Stx-induced complications. Thus we showed here that inhibition of NMII and Cdc42 by either pharmacological or molecular approaches significantly decreased EHEC-stimulated Stx1 uptake and transcytosis. Particularly interesting from the potential therapeutic point of view is the inhibition of toxin uptake by NHE inhibitors, including these inhibiting NHE2, a major apical NHE in human colonocytes. Although never used orogastrally, several of such compounds including HOE-694 have already been used in animal studies of cardiac ischemia and cardiomyopathy (3, 31). Further *in vivo* studies using the relevant animal models of human EHEC infection should be carried out to test the effectiveness

of inhibiting MPC on the outcome of EHEC-induced intestinal and systemic complications.

In conclusion, we identified and characterized a novel mechanism of Stx1 and Stx2 uptake by human IEC for which the EHEC infection is a necessary stimulus. In the absence of any therapeutics to interfere with Stx-caused systemic and intestinal damages, the inhibition of EHEC-stimulated MPC of toxin, as we showed here, may provide an attractive, antibiotic-independent strategy to diminish the harmful consequences of EHEC infection.

ACKNOWLEDGMENTS

We acknowledge the Johns Hopkins Ross Confocal Facility and the image processing assistance of Mr. John Gibas.

GRANTS

This work was supported by National Institutes of Health Grants RO1DK-58928 (OK), T32DK-2007632 (VL and IM) and R24DK-064388 (OK and AH).

DISCLOSURES

No conflicts of interest, financial or otherwise, are declared by the author(s).

REFERENCES

- Acheson DWK, Donohue-Rolfe A, Keusch GT. The family of Shiga and Shiga-like toxins. In *Sourcebook of Bacterial Protein Toxin* edited by Aloufand JE and Freer JH. London, UK: Academic, 1991, p. 415–433.
- Acheson DW, Moore R, De Breucker S, Lincicome L, Jacewicz M, Skutelsky E, Keusch GT. Translocation of Shiga toxin across polarized intestinal cells in tissue culture. *Infect Immun* 64: 3294–3300, 1996.
- Avkiran M. Rational basis for use of sodium-hydrogen exchange inhibitors in myocardial ischemia. *Am J Cardiol* 83: 10G–18G, 1999.
- Beltrán AR, Ramírez MA, Carraro-Lacroix LR, Hiraki Y, Rebouças NA, Malnic G. NHE1, NHE2, and NHE4 contribute to regulation of cell pH in T84 colon cancer cells. *Pflügers Arch* 455: 799–810, 2008.
- Björk S, Breimer ME, Hansson GC, Karlsson KA, Leffler H. Structures of blood group glycosphingolipids of human small intestine. A relation between the expression of fucolipids of epithelial cells and the ABO, Le and Se phenotype of the donor. *J Biol Chem* 262: 6758–6765, 1987.
- Caron E, Crepin VF, Simpson N, Knutton S, Garmendia J, Frankel G. Subversion of actin dynamics by EPEC and EHEC. *Curr Opin Microbiol* 9: 40–45, 2006.
- Center for Disease Control, and Prevention. Ongoing multistate outbreak of *Escherichia coli* serotype O157:H7 infections associated with consumption of fresh spinach—United States, September 2006. *MMWR Morb Mortal Wkly Rep* 55: 1045–1046, 2006.
- Chun J, Prince A. TLR2-induced calpain cleavage of epithelial junctional proteins facilitates leukocyte transmigration. *Cell Host Microbe* 5: 47–58, 2009.
- Conti MA, Adelstein RS. Nonmuscle myosin II moves in new directions. *J Cell Sci* 121: 11–18, 2008.
- Croxen MA, Finlay BB. Molecular mechanisms of *Escherichia coli* pathogenicity. *Nat Rev Microbiol* 8: 26–38, 2010.
- Donaldson JG, Porat-Shliom N, Cohen LA. Clathrin-independent endocytosis: a unique platform for cell signaling and PM remodeling. *Cell Signal* 21: 1–6, 2009.
- Falcone S, Cocucci E, Podini P, Kirchhausen T, Clementi E, Meldolesi J. Macropinocytosis: regulated coordination of endocytic and exocytic membrane traffic events. *J Cell Sci* 119: 4758–4769, 2006.
- Garred O, van Deurs B, Sandvig K. Furin-induced cleavage and activation of Shiga toxin. *J Biol Chem* 270: 10817–10821, 1995.
- Garrett WS, Chen LM, Kroschewski R, Ebersold M, Turley S, Trombetta S, Galán JE, Mellman I. Developmental control of endocytosis in dendritic cells by Cdc42. *Cell* 102: 325–334, 2000.
- Harris Tepass KP, U. Cdc42 and vesicle trafficking in polarized cells. *Traffic* 11: 1272–1279, 2010.
- Heasman SJ, Ridley AJ. Mammalian Rho GTPases: new insights into their functions from in vivo studies. *Nat Rev Mol Cell Biol* 9: 690–701, 2008.
- Hecht G, Hodges K, Gill RK, Kear F, Tyagi S, Malakooti J, Ramaswamy K, Dudeja PK. Differential regulation of Na⁺/H⁺ exchange isoform activities by enteropathogenic *E. coli* in human intestinal epithelial cells. *Am J Physiol Gastrointest Liver Physiol* 287: G370–G378, 2004.
- Holgerson J, Jovell PA, Breimer ME. Glycosphingolipids of the human large intestine: detailed structural characterization with special reference to blood group compounds and bacterial receptor structures. *J Biochem (Tokyo)* 110: 120–131, 1991.
- Hurley BP, Jacewicz M, Thorpe CM, Lincicome LL, King AJ, Keusch GT, Acheson DW. Shiga toxins 1 and 2 translocate differently across polarized intestinal epithelial cells. *Infect Immun* 67: 6670–6677, 1999.
- Hurley BP, Thorpe CM, Acheson DW. Shiga toxin translocation across intestinal epithelial cells is enhanced by neutrophil transmigration. *Infect Immun* 69: 61 48–55, 2001.
- Ivanov AI, McCall IC, Parkos CA, Nusrat A. Role for actin filament turnover and a myosin II motor in cytoskeleton-driven disassembly of the epithelial apical junctional complex. *Mol Biol Cell* 15: 2639–2651, 2004.
- Jiang J, Kolpak AL, Bao ZZ. Myosin IIB isoform plays an essential role in the formation of two distinct types of macropinosomes. *Cytoskeleton* 67: 32–42, 2010.
- Johannes L, Römer W. Shiga toxins—from cell biology to biomedical applications. *Nat Rev Microbiol* 8: 105–116, 2010.
- Kasahara K, Nakayama Y, Sato I, Ikeda K, Hoshino M, Endo T, Yamaguchi N. Role of Src-family kinases in formation and trafficking of macropinosomes. *J Cell Physiol* 211: 220–232, 2007.
- Kerr MC, Teasdale RD. Defining macropinocytosis. *Traffic* 10: 364–371, 2009.
- Koivusalo M, Welch C, Hayashi H, Scott CC, Kim M, Alexander T, Touret N, Hahn KM, Grinstein S. Amiloride inhibits macropinocytosis by lowering submembranous pH and preventing Rac1 and Cdc42 signaling. *J Cell Biol* 188: 547–563, 2010.
- Kovbasnjuk O, Mourtzina R, Baibakov B, Wang T, Elowsky C, Choti MA, Kane A, Donowitz M. The glycosphingolipid globotriaosylceramide in the metastatic transformation of colon cancer. *Proc Natl Acad Sci USA* 102: 19087–19092, 2005.
- Kurmanova A, Llorente A, Poleskaya A, Garred O, Olsnes S, Kozlov J, Sandvig K. Structural requirements for furin-induced cleavage and activation of Shiga toxin. *Biochem Biophys Res Commun* 357: 144–149, 2007.
- Laiko M, Murtazina R, Malyukova I, Zhu C, Boedeker EC, Gutsal O, O'Malley R, Cole RN, Tarr PI, Murray KF, Kane A, Donowitz M, Kovbasnjuk O. Shiga toxin 1 interaction with enterocytes causes apical protein mistargeting through the depletion of intracellular galectin-3. *Exp Cell Res* 316: 657–666, 2010.
- Lee CS, Choi CK, Shin EY, Schwartz MA, Kim EG. Myosin II directly binds and inhibits Dbl family guanine nucleotide exchange factors: a possible link to Rho family GTPases. *J Cell Biol* 190: 663–674, 2010.
- Liu H, Cala PM, Anderson SE. Na/H exchange inhibition protects newborn heart from ischemia/reperfusion injury by limiting Na⁺-dependent Ca²⁺ overload. *J Cardiovasc Pharmacol* 55: 227–233, 2010.
- Malyukova I, Gutsal O, Laiko M, Kane A, Donowitz M, Kovbasnjuk O. Latrunculin B facilitates Shiga toxin 1 transcellular transcytosis across T84 intestinal epithelial cells. *Biochim Biophys Acta* 1782: 370–377, 2008.
- Malyukova I, Murray KF, Zhu C, Boedeker E, Kane A, Patterson K, Peterson JR, Donowitz M, Kovbasnjuk O. Macropinocytosis in Shiga toxin 1 uptake by human intestinal epithelial cells and transcellular transcytosis. *Am J Physiol Gastrointest Liver Physiol* 296: G78–G92, 2009.
- Matsumara F. Regulation of myosin II during cytokinesis in higher eukaryotes. *Trends Cell Biol* 15: 371–377, 2005.
- Mercer J, Helenius A. Virus entry by macropinocytosis. *Nat Cell Biol* 11: 510–520, 2009.
- Mettlen M, Platek A, Van Der Smissen P, Carpentier S, Amyere M, Lanzetti L, de Diesbach P, Tyteca D, Courtoy PJ. Src triggers circular ruffling and macropinocytosis at the apical surface of polarized MDCK cells. *Traffic* 7: 589–603, 2006.
- Pelish HE, Ciesla W, Tanaka N, Reddy K, Shair MD, Kirchhausen T, Lencer WI. The Cdc42 inhibitor secriamine B prevents cAMP-induced K⁺ conductance in intestinal epithelial cells. *Biochem Pharmacol* 71: 1720–1726, 2006.
- Ragnarsson EG, Schoultz I, Gullberg E, Carlsson AH, Tafazoli F, Lerm M, Magnusson KE, Söderholm JD, Artursson P. Yersinia pseudotuberculosis induces transcytosis of nanoparticles across human intestinal villus epithelium via invasin-dependent macropinocytosis. *Lab Invest* 88: 1215–1226, 2008.

39. Robles E, Woo S, Gomez TM. Src-dependent tyrosine phosphorylation at the tips of growth cone filopodia promotes extension. *J Neurosci* 25: 7669–7681, 2005.
40. Roxas JL, Koutsouris A, Bellmeyer A, Tesfay S, Royan S, Falzari K, Harris A, Cheng H, Rhee KJ, Hecht G. Enterohemorrhagic E coli alters murine intestinal epithelial tight junction protein expression and barrier function in a Shiga toxin independent manner. *Lab Invest* 90: 1152–1168, 2010.
41. Sal-Man N, Biemans-Oldehinkel E, Finlay BB. Structural microengineers: pathogenic *Escherichia coli* redesign the actin cytoskeleton in host cells. *Structure* 17: 15–19, 2009.
42. Sandvig K, Van Deurs B. Endocytosis, intracellular transport, and cytotoxic action of Shiga toxin and ricin. *Physiol Rev* 76: 949–966, 1996.
43. Schuller S, Frankel G, Phillips AD. Interaction of Shiga toxin from *Escherichia coli* with human intestinal epithelial cell lines and explants: Stx2 induces epithelial damage in organ culture. *Cell Microbiol* 6: 289–301, 2004.
44. Schwark JR, Jansen HW, Lang HJ, Krick W, Burckhardt G, Hropot M. S3226, a novel inhibitor of Na⁺/H⁺ exchanger subtype 3 in various cell types. *Pflügers Arch* 436: 797–800, 1998.
45. Serna, A 4th, Boedeker EC. Pathogenesis and treatment of Shiga toxin-producing *Escherichia coli* infections. *Curr Opin Gastroenterol* 24: 38–47, 2008.
46. Sherman A, Philpott DJ, Ackerley CA, Kiliaan AJ, Karmali MA, Perdue MH, Sherman PM. Translocation of verotoxin-1 across T84 monolayers: mechanism of bacterial toxin penetration of epithelium. *Am J Physiol Gastrointest Liver Physiol* 273: G1349–G1358, 1997.
47. Sjogren R, Neill R, Rachmilewitz D, Fritz D, Newland J, Sharpnack D, Colleton C, Fondacaro J, Gemski P, Boedeker E. Role of Shiga-like toxin I in bacterial enteritis: comparison between isogenic *Escherichia coli* strains induced in rabbits. *Gastroenterology* 106: 306–317, 1994.
48. Straight AF, Cheung A, Limouze J, Chen I, Westwood NJ, Sellers JR, Mitchison TJ. Dissecting temporal and spatial control of cytokinesis with a myosin II Inhibitor. *Science* 299: 1743–1747, 2003.
49. Swanson JA. Shaping cups into phagosomes and macropinosomes. *Nat Rev Mol Cell Biol* 9: 639–649, 2008.
50. Swanson JA, Watts C. Macropinocytosis. *Trends Cell Biol* 5: 424–428, 1995.
51. Tarr PI, Gordon CA, Chandler WL. Shiga-toxin-producing *Escherichia coli* and haemolytic uraemic syndrome. *Lancet* 365: 1073–1086, 2005.
52. Tu X, Nisan I, Yona C, Hanski E, Rosenshine I. EspH, a new cytoskeleton-modulating effector of enterohaemorrhagic and enteropathogenic *Escherichia coli*. *Mol Microbiol* 47: 595–606, 2003.
53. Vastrik I, Eickholt BJ, Walsh FS, Ridley A, Doherty P. Sema3A-induced growth-cone collapse is mediated by Rac1 amino acids 17–32. *Curr Biol* 9: 991–998, 1999.
54. Wilson CA, Tsuchida MA, Allen GM, Barnhart EL, Applegate KT, Yam PT, Ji L, Keren K, Danuser G, Theriot JA. Myosin II contributes to cell-scale actin network treadmill through network disassembly. *Nature* 465: 373–377, 2010.
55. Wong CS, Jelacic S, Habeeb RL, Watkins SL, Tarr PI. The risk of the hemolytic-uremic syndrome after antibiotic treatment of *Escherichia coli* O157:H7 infections. *N Engl J Med* 342: 1930–1936, 2000.
56. Yoshida S, Hoppe AD, Araki N, Swanson JA. Sequential signaling in plasma-membrane domains during macropinosome formation in macrophages. *J Cell Sci* 122: 3250–3261, 2009.
57. Zumbrun SD, Hanson L, Sinclair JF, Freedy J, Melton-Celsa AR, Rodriguez-Canales J, Hanson JC, O'Brien AD. Human intestinal tissue and cultured colonic cells contain globotriaosylceramide synthase mRNA and the alternate Shiga toxin receptor globotetraosylceramide. *Infect Immun* 78: 4488–4499, 2010.

